J Mater Sci: Mater Electron (2018) 29:2874–2882
DOI 10.1007/s10854-017-8217-3

Microstructure and optoelectronic properties of gallium–magnesium codoped zinc oxide thin films by magnetron sputtering technique

H. Kang[1] · Z. Lu[1] · Z. Zhong[1] · T. Zhang[1]

Received: 24 July 2017 / Accepted: 6 November 2017 / Published online: 11 November 2017
© Springer Science+Business Media, LLC, part of Springer Nature 2017

Abstract The gallium–magnesium codoped zinc oxide (GMZO) thin films were deposited on glass substrates by radio frequency magnetron sputtering technique in an argon atmosphere. The influence of substrate temperature on the microstructure, morphology and optoelectronic properties of thin films was investigated by X-ray diffraction, scanning electron microscopy, X-ray photoelectron spectroscopy, four-point probe and spectrophotometry. It is found that all the deposited films have a hexagonal structure and a preferred orientation along the *c*-axis perpendicular to the substrate. As the substrate temperature increases, the dislocation density, lattice strain and electrical resistivity decrease initially and then increase, while the average crystallite size, average visible transmittance and figure of merit exhibit the reverse variation trend. The GMZO thin film deposited at the substrate temperature of 570 K possesses the best optoelectronic properties, with the largest average crystallite size of 52.05 nm, the lowest dislocation density of 3.69×10^{14} lines m^{-2}, the minimum lattice strain of 1.10×10^{-3}, the lowest electrical resistivity of $1.62\times10^{-3}\ \Omega$ cm, the highest average visible transmittance of 88.63% and the maximum figure of merit of $5.11\times10^{3}\ \Omega^{-1}\ cm^{-1}$. The optical energy gaps of the films were evaluated by extrapolation method and observed to be in the range of 3.34–3.55 eV. Furthermore, the complex refractive index, the complex dielectric constant and the dissipation factor were determined by optical characterization methods, and the dispersion behaviour of refractive index was studied in terms of the single electronic oscillator model. The results show that the microstructure and optoelectronic properties of the GMZO thin films are dependent on substrate temperature.

✉ H. Kang
csbillion@163.com

✉ Z. Zhong
longscun@163.com

[1] College of Electronic Information Engineering, Hubei Key Laboratory of Intelligent Wireless Communications, South-Central University for Nationalities, Wuhan 430073, China

1 Introduction

Transparent conductive oxides (TCOs) play an important role in optoelectronic devices including solar cells [1, 2], flat panel displays [3, 4], thin film transistors [5], light emitting diodes [6, 7] and chemical sensors [8–10], etc. It is well known that tin-doped indium oxide (ITO) is the most widely used TCO film due to its high transparency, low resistivity and high work function [11]. However, taking into account the high cost due to the scarcity of indium, other alternative TCO materials have been explored extensively. Among these materials, zinc oxide (ZnO) is nontoxic, inexpensive and offers good chemical stability in strong hydrogen plasma atmosphere. The ZnO-based TCOs with Ga, Al, or other group III elements have been steadily investigated due to high transparency and electrical conductivity. Recently, a variety of techniques have been introduced to improve electrical and optical properties for ZnO-based TCOs. Especially, codoping with solute atoms is an effective method to improve various properties of ZnO for TCO. Up to now, the Ga–In, In–Al, V–Al, Al–Ga, Al–Ti, B–Ga, Mg–Al and Ga–Ti codoping cases have been reported [12–19]. Different technologies such as chemical vapor deposition [20], molecular beam epitaxy [21], sol–gel [22, 23], chemical spray [24, 25], magnetron sputtering [26–30] and pulsed laser deposition [31], have been utilized to prepare the codoped ZnO thin films with adequate performance for applications. Among the deposition techniques, radio frequency (RF) magnetron

sputtering technique has some advantages in comparison with the other methods. This technique is quite simple and the required setup is less expensive, and it is considered to be the most available deposition method to obtain highly uniform films with high packing density and strong adhesion at a high deposition rate [32, 33]. To our knowledge, although many experimental studies have been conducted on the synthesis and electrical properties of codoped ZnO films, there are no detailed studies on their refractive index and dispersion behaviour, which are important parameters for TCO thin films. In this present work, Ga–Mg codoped ZnO (GMZO) TCO films were deposited on glass substrates by radio frequency (RF) magnetron sputtering technique at different substrate temperatures. The influence of substrate temperature on microstructure and optoelectronic properties of the thin films was investigated in detail.

2 Experimental details

The GMZO samples were deposited on the cleaned glass substrates by using RF magnetron sputtering equipment (KDJ-567). A sintered GMZO ceramic sputter target (2 wt.% Ga_2O_3: 2 wt.% MgO: 96 wt.% ZnO, 99.99% purity) was employed as source material. The sputtering chamber was evacuated to a base pressure below 3.0×10^{-4} Pa before argon gas. After vacuum pumping, the sputtering argon gas with a purity of 99.999% was introduced into the chamber and controlled by the standard mass flow controllers. Before the GMZO samples deposition, pre-sputtering was conducted for about 10 min to attain stability and to remove impurities. The deposition parameters for preparing GMZO samples were as follows: substrate-target distance, 75 mm; sputtering power, 135 W; operating pressure, 3 Pa; and sputtering time, 45 min. In order to investigate the influence of substrate temperature (T_s) on properties of the GMZO thin films, the substrate temperature was changed from 370 to 670 K. The thickness of the samples was measured by a surface profiler (Alpha-step 500). X-ray diffraction studies were conducted to determine the crystal structure with a D8-Advance diffractometer in the θ–2θ configuration using Cu Kα radiation ($\lambda=0.15406$ nm) at 40 kV and 40 mA. The surface morphology was observed using a scanning electron microscope (SEM, JSM-6700F). The chemical composition was determined by an X-ray photoelectron spectroscopy (XPS, VG Multilab 2000) with Al Kα X-ray source ($h\nu=1486.6$ eV) at constant analyzer pass energy of 25 eV. The C 1s line (284.6 eV) was taken as a reference to correct for electrostatic charging. The electrical properties were evaluated using a four-point probe measurement system (RH-2035). The optical transmittance spectra were recorded with a double-beam ultraviolet–visible (UV–Vis) spectrophotometer (TU-1901), and the optical constants of samples were determined from the transmittance data using the method of optical spectrum fitting [34, 35]. All measurements were performed at room temperature in ambient air.

3 Results and discussion

Figure 1 presents the XRD patterns of GMZO samples deposited at different substrate temperatures. These XRD peaks are assigned to ZnO according to the Joint Committee of Powder Diffraction Standards Card (JCPDS 36-1451). Note that all the samples exhibit a dominant (002) peak with slight (004) peak in the displayed 2θ region, which indicates that the GMZO thin films have highly preferred orientation with their crystallographic *c*-axis perpendicular to the substrates, irrespective of substrate temperature. Note also that neither metallic Ga or Mg characteristic peaks nor Ga_2O_3 or MgO peaks was observed from the XRD patterns, which implies that the dopants have not destroyed the ZnO structure and act as typical dopants. Similar results have been reported by many researchers [29, 36, 37].

Figure 2 shows the intensity of (002) peak ($I_{(002)}$) and the intensity ratio of (004) to (002) ($I_{(004)}/I_{(002)}$) for GMZO samples deposited at different substrate temperatures. Corresponding to the substrate temperatures of 370, 470, 570 and 670 K, the values of $I_{(002)}$ and $I_{(004)}/I_{(002)}$ for the samples are found to be 9.72×10^3 cps, 3.47%; 2.60×10^4 cps, 2.13%; 4.63×10^4 cps, 1.97%; and 2.98×10^4 cps, 2.11%, respectively. With the increment of substrate temperature, the $I_{(002)}$ increases initially and then decreases, but the $I_{(004)}/I_{(002)}$ takes on an opposite trend. The GMZO sample prepared at the substrate temperature of 570 K has the maximum $I_{(002)}$ and the minimum $I_{(004)}/I_{(002)}$, which indicates that the deposited film possesses the best preferred (002) orientation.

Figure 3a displays the full-width at half-maximum (β) values of (002) peak of GMZO samples deposited at

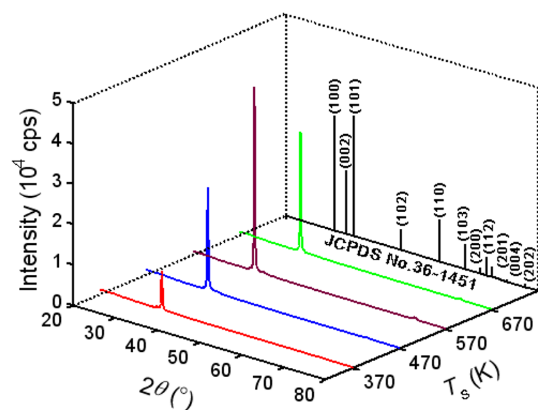

Fig. 1 XRD patterns of the films deposited at different substrate temperatures

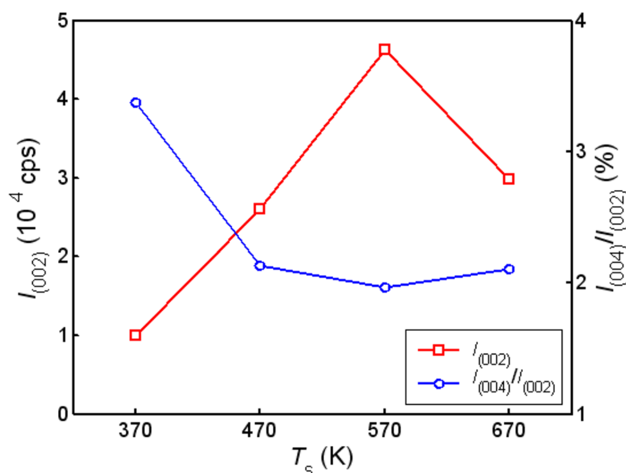

Fig. 2 The values of $I_{(002)}$ and $I_{(004)}/I_{(002)}$ for the films deposited at different substrate temperatures

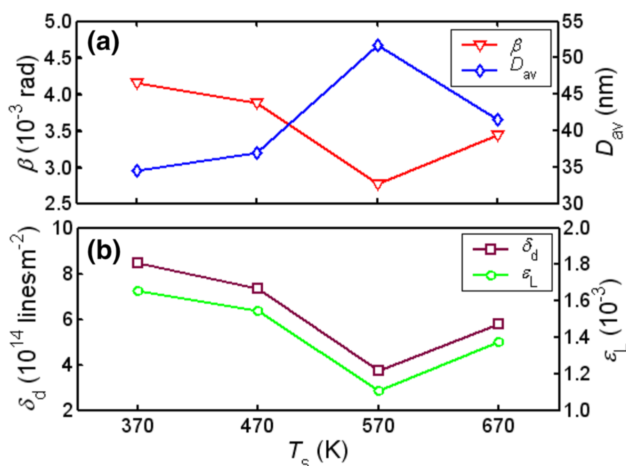

Fig. 3 The values of β, D, δ_d and ε for the films deposited at different substrate temperatures

different substrate temperatures. As can be seen, the β falls firstly and then rises with the increase of substrate temperature, and the minimum β of 2.76×10^{-3} rad can be achieved when the substrate temperature is at 570 K. The decrease of the β indicates the increase of average crystallite size (D_{av}) of the deposited films. The D_{av} values of the samples can be evaluated from β data according to the Scherrer equation [38, 39]:

$$D_{av} = K\frac{\lambda}{\beta\cos\theta} \tag{1}$$

Where K is the Scherrer constant dependent on crystallite shape and can be considered as 0.89, λ is the wavelength of X-rays used, β is the full-width at half-maximum, and θ is the Bragg's diffraction angle at peak position. The dislocation density (δ_d) and the lattice strain (ε_L) can be estimated from the following formulae [40, 41]:

$$\delta_d = \frac{1}{D_{av}^2} \tag{2}$$

$$\varepsilon_L = \frac{\lambda}{D_{av}\sin\theta} - \beta\cot\theta \tag{3}$$

where D_{av} is the average crystallite size, β is the full-width at half-maximum, and θ is the Bragg's diffraction angle. The results of D_{av}, δ_d and ε_L of all the deposited samples were calculated and are plotted in Fig. 3a, b, respectively. From Fig. 3a, we note that the D_{av} value increases with the substrate temperature increasing from 370 to 570 K, reaches to the maximum value of 52.05 nm at 570 K, and thereafter decreases to 41.32 nm at 670 K. An opposite trend is observed in both δ_d and ε_L of the samples as shown in Fig. 3b. When the substrate temperature is 570 K, the deposited GMZO sample exhibits the best crystalline and microstructural properties, with the narrowest β of 2.76×10^{-3} rad, the largest D_{av} of 52.05 nm, the minimum δ_d of 3.69×10^{14} lines m^{-2} and the lowest ε_L of 1.10×10^{-3}. The results suggest that the crystal quality of the GMZO thin films is strongly dependent upon the substrate temperature.

Figure 4a–d give the SEM images of GMZO samples deposited at substrate temperatures of 370, 470, 570 and 670 K, respectively. From the SEM micrographs, it can be seen that the deposited films consist of some columnar structured and *c*-axis oriented grains. The surfaces of the thin films are observed to be smooth, and the grains are homogeneously distributed. Note also that the substrate temperature greatly affects the surface structure of the deposited films. The morphologies of thin films prepared at lower substrate temperature are found to be continuous and dense. With the substrate temperature increasing to 570 K, the crystalline quality of deposited film is improved and the grain size evidently grows larger. Above the substrate temperature of 570 K, yet, the grain size of the film becomes slightly smaller than that of film deposited at 570 K. The evolution of microstructure could be attributed to the migration of surface atoms during the deposition process. At low substrate temperature, the sputtered atoms possess less energy and low surface mobility. With the increase of the substrate temperature, these atoms have sufficient energy and surface mobility to settle in stable position. This gives rise to the most stable *c*-axis oriented structure as preferred growth orientation, and thus the denser film with larger grains and lower defects can be obtained. However, further increase of energy in the case of higher substrate temperature (>570 K) results in the breaking of the Zn–O bond and the re-evaporation of the deposited film rather than enabling the atoms to move to

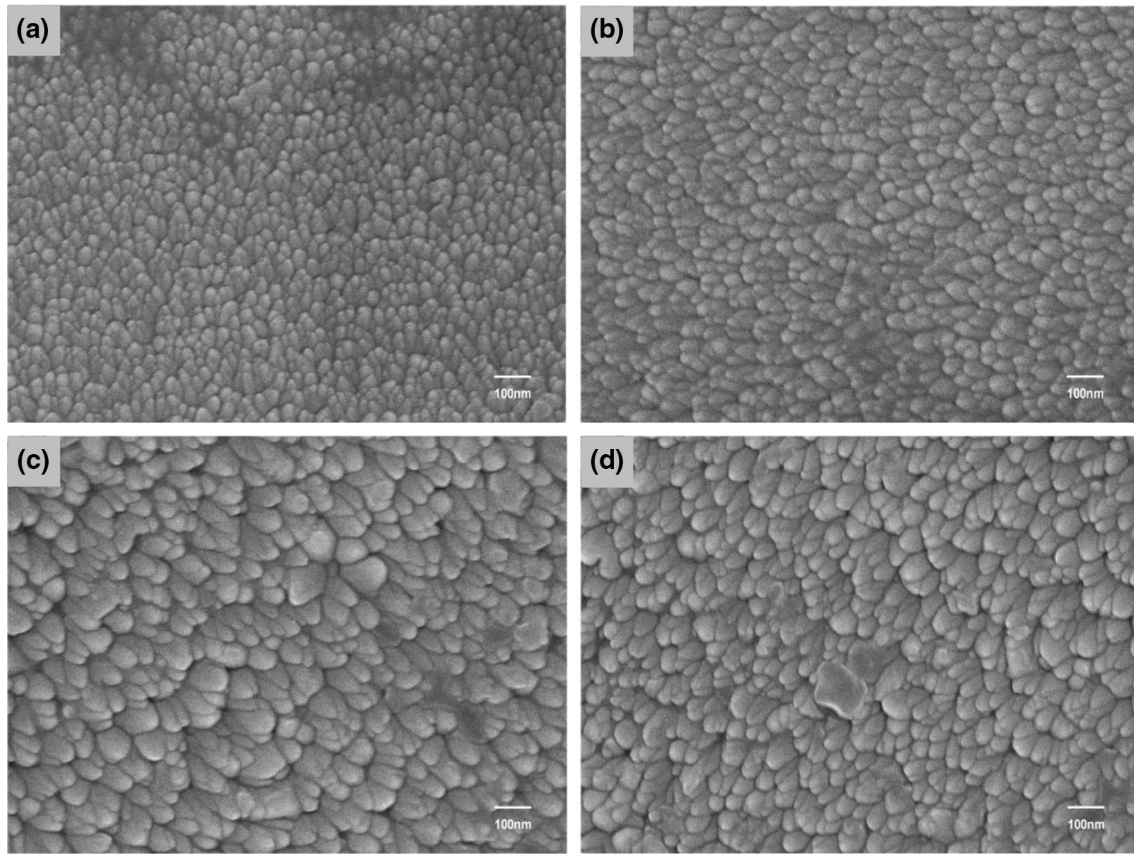

Fig. 4 SEM images of the films deposited at **a** 370 K, **b** 470 K, **c** 570 K and **d** 670 K

their stable sites, and then the crystallinity is deteriorated. The SEM observations are in agreement with the XRD results.

The XPS spectra of GMZO samples deposited at different substrate temperatures are shown in Fig. 5, where photoelectron peaks of Ga, Mg, Zn, O and C are detected. The peaks at about 1117.8, 1021.5, 530.0, 50.2 eV corresponds to Ga $2p_{3/2}$, Zn $2p_{3/2}$, O1s and Mg 2p, respectively. The carbon residues appear to come from the contamination during sample preparation and measurement. The elemental composition of the deposited films was calculated using the following formula [42]:

$$[\mathrm{X}] = \left(\frac{A_{\mathrm{X}}}{S_{\mathrm{X}}}\right) \Big/ \sum_{i=1}^{N} \left(\frac{A_{\mathrm{X}}}{S_{\mathrm{X}}}\right) \tag{4}$$

where [X] is the content of element X, A_{X} is the area under the peak of element X in the spectrum, and S_{X} is the sensitivity factor [43]. The values of [Ga] and [Mg] for the deposited films were calculated and are plotted in the inset of Fig. 5 as a function of substrate temperature. Note that for the GMZO samples prepared at the substrate temperatures of 370, 470, 570 and 670 K, the Ga contents are 1.02, 1.06, 1.18 and

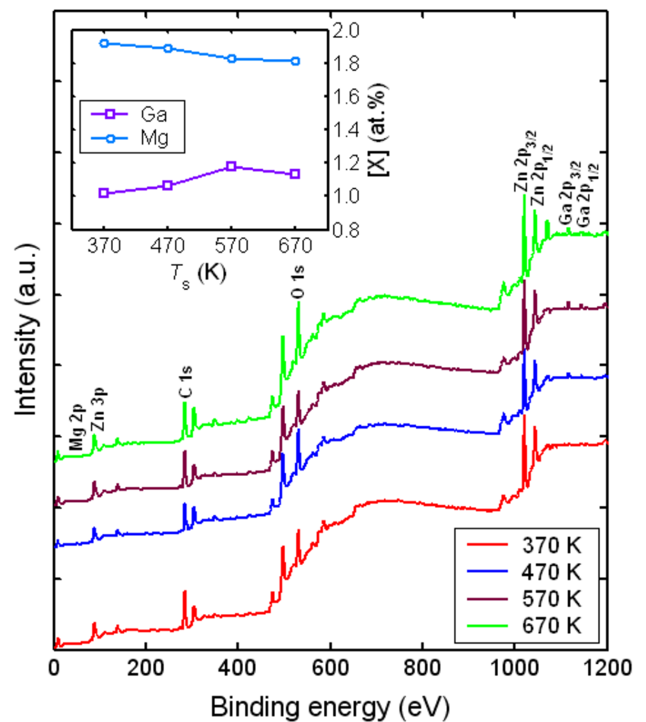

Fig. 5 XPS spectra of the films deposited at different substrate temperatures

1.13 at.%, and the corresponding Mg contents are 1.92, 1.89, 1.83 and 1.81 at.%, respectively. The results indicate that the chemical composition of the deposited films is affected slightly by substrate temperature.

The optical transmission spectra of all the samples deposited on glass substrates were measured by UV–Vis spectrophotometer, using the glass substrate as reference. Figure 6 shows the optical transmittance (*T*) curves of GMZO films prepared at different substrate temperatures. As can be seen, all the transmission spectra show interference pattern with sharp fall of transmittance near the band edge, which is an indication of good crystallinity. As shown in the inset of Fig. 6, the average visible transmittance (T_{av}) increases slightly with the substrate temperature up to 570 K, and then significantly decreases when the substrate temperature is over 570 K. The highest T_{av} value of 88.63% for the GMZO film can be achieved at the substrate temperature of 570 K. This enhancement in the optical transmittance is closely related to the increase of crystallite size and the improvement of crystallinity of the deposited thin films. Near the absorption edge of the transmittance spectra, the absorption coefficient (α) is related to the optical energy gap (E_g) following the power-law behaviour of Tauc relation [44, 45]:

$$(\alpha E)^p = C\left(E - E_g\right), \quad (5)$$

where E is the photon energy, C is an energy-independent constant, and p is an index which can assume values of 1/3, 1/2, 2/3 and 2 depending on the nature of the electronic transitions responsible for the optical absorption ($p=2$ and 2/3 for direct allowed and forbidden transitions, respectively, $p=1/2$ and 1/3 for indirect allowed and forbidden transition, respectively) [46, 47]. Figure 7 presents the Tauc plots of $(\alpha E)^2$ versus E for GMZO samples deposited at different

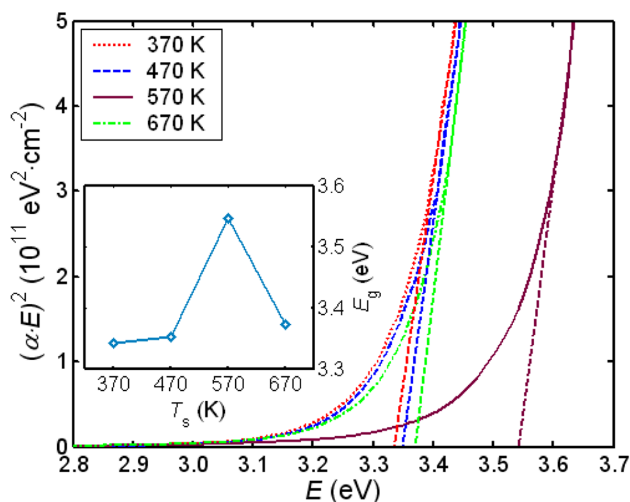

Fig. 7 The curves of $(\alpha E)^2$ versus E for the films deposited at different substrate temperatures

substrate temperatures. The values of E_g for the deposited films can be estimated by extrapolating the straight line portion of the curves to the energy axis [48, 49], and are summarized in the inset of Fig. 7 as a function of substrate temperature. As can be seen, the E_g values of GMZO samples are in the range of 3.34–3.55 eV, larger than that of pure ZnO (3.30 eV). The widening of optical energy gap may be attributed to Moss–Burstein shift [50, 51] in which the absorption edge shifts towards higher energy with an increase of carrier concentration. Similar results have been reported in the previously literatures [52–55].

Figure 8 displays the electrical resistivity (ρ) of GMZO samples deposited at different substrate temperatures. As the substrate temperature increases from 370 to 570 K, ρ

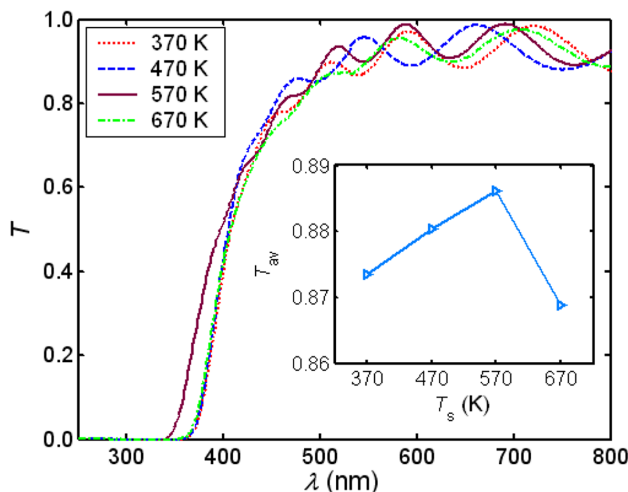

Fig. 6 Transmittance curves of the films deposited at different substrate temperatures

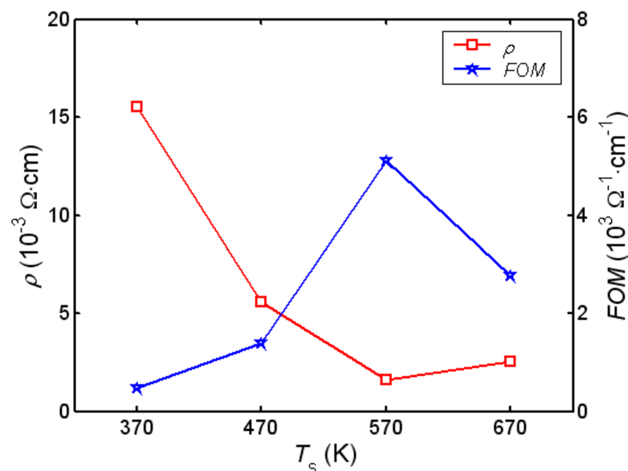

Fig. 8 The values of ρ and *FOM* for the films deposited at different substrate temperatures

drops initially and subsequently rises beyond the temperature of 570 K. The lowest ρ value of $1.62 \times 10^{-3}\ \Omega$ cm is obtained for the GMZO thin film deposited at the substrate temperature of 570 K. The reduction in the electrical resistivity can be attributed to the increase of crystallite size and the improvement of crystallinity [56], which is confirmed by the results of XRD discussed above. As we all know, an increase in the crystallite size can cause a decrease in grain-boundary scattering and an increase in carrier lifetime, and consequently lead to an increase in both the carrier concentration and Hall mobility, and hence result in a decrease in resistivity [57]. When the substrate temperature increases from 370 to 570 K, the crystallite size increases obviously and the grain boundaries decrease rapidly, and thereby the resistivity decreases sharply. With further increasing the substrate temperature from 570 to 670 K, however, the crystallite size decreases and the grain boundaries increase, and accordingly the electrical resistivity increases. The results suggest that the substrate temperature is one of the most important factors to affect the electrical properties of GMZO thin films.

In order to evaluate the quality of the deposited TCO thin films, the figure of merit (*FOM*) is given by the following formula [58, 59]:

$$FOM = -\frac{1}{\rho \log\left(T_{av}\right)} \tag{6}$$

Where ρ is the electrical resistivity, and T_{av} is the average visible transmittance. Figure 8 shows the variation of *FOM* versus the substrate temperature for the deposited GMZO samples. As the substrate temperature increases, the *FOM* increases firstly and then decreases and reaches its maximum value of $5.11 \times 10^3\ \Omega^{-1}\ \mathrm{cm}^{-1}$ at the substrate temperature of 570 K. The increase in *FOM* with substrate temperature was due to increase in optical transmittance and decrease in the electrical resistivity. It is known that the higher the *FOM*, the better quality of the TCO thin film. Thus, in this study, it can be concluded that the optimum substrate temperature is 570 K, where the *FOM* value is the highest.

From the measured optical transmittance data, the optical constants including refractive index (n) and extinction coefficient (k) of the deposited samples were determined using the method of optical spectrum fitting [34, 35]. Figure 9 shows the k and n of the deposited films as a function of wavelength (λ). As can be seen, the k values of the samples are very small at long wavelengths, indicating that the deposited films are highly transparent. In addition, the curves of the k are fairly flat above 420 nm and rise rapidly at shorter wavelength λ. Similar to the curves of the k, the n decrease monotonically with increasing λ for the deposited films, indicating the typical shape of the dispersion curve near an electronic interband transition. For the GMZO samples prepared at the substrate temperatures of 370, 470, 570 and 670 K, the n values are 2.074–1.817, 2.038–1.809, 1.998–1.801 and 1.924–1.786, and the corresponding k values are 3.282×10^{-2}–8.283×10^{-5}, 3.151×10^{-2}–6.258×10^{-5}, 2.194×10^{-2}–2.575×10^{-4} and 3.305×10^{-2}–3.345×10^{-4} respectively in the visible range. The results in our present work are in agreement with the other works [60–62].

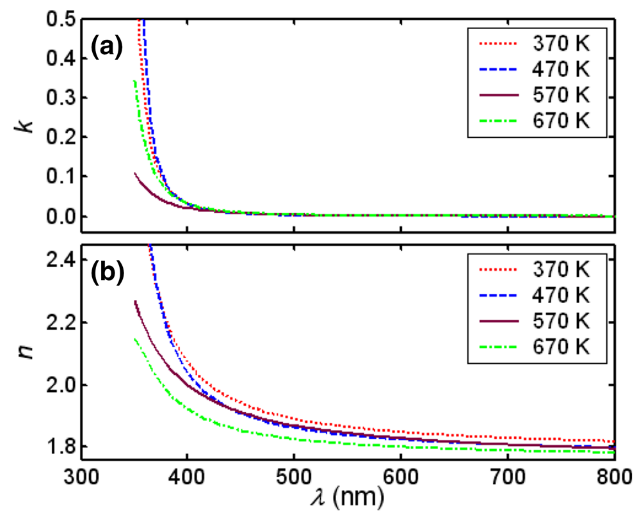

Fig. 9 The curves of k and n for the films deposited at different substrate temperatures

The refractive index $n(\lambda)$ data of the deposited films were analyzed by the single electronic oscillator model [63]:

$$\frac{1}{[n(\lambda)]^2 - 1} = -\frac{1}{S_o\lambda^2} + \frac{1}{S_o\lambda_o^2}, \tag{7}$$

where S_o is the average oscillator strength, and λ_o is the average oscillator position. The curves of $(n^2 - 1)^{-1}$ versus λ^{-2} for GMZO samples deposited at different substrate temperatures are plotted in Fig. 10 and the data are fitted into straight lines. The results indicate that the single electronic oscillator model is applicable to the GMZO thin films in our work.

The complex dielectric constant (ε) is an important optical parameter that helps to describe the response of a crystal to an electromagnetic field. The complex dielectric constant ε is defined as:

$$\varepsilon = \varepsilon_1 + i\varepsilon_2 \tag{8}$$

where ε_1 and ε_2 are real and imaginary parts of the complex dielectric constant ε, respectively. These values were determined by using the following relations [64]:

$$\varepsilon_1 = n^2 - k^2,\ \varepsilon_2 = 2nk \tag{9}$$

The variation of ε_1 and ε_2 with wavelength λ for GMZO samples deposited at different substrate temperatures is shown in Fig. 11. Note that both ε_1 and ε_2 tend to

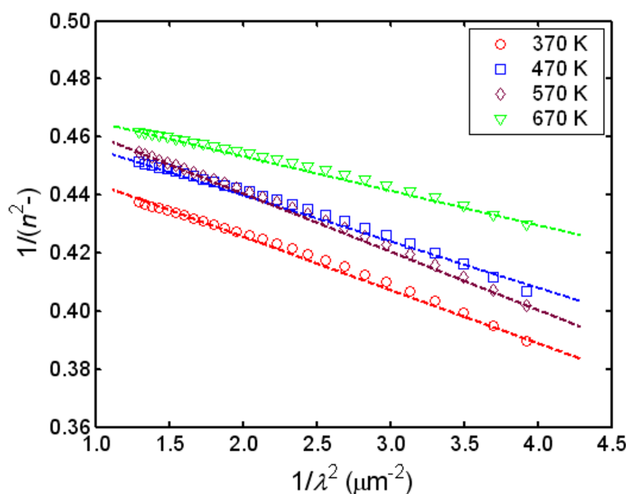

Fig. 10 The curves of $1/(n^2-1)$ versus $1/\lambda^2$ for the films deposited at different substrate temperatures

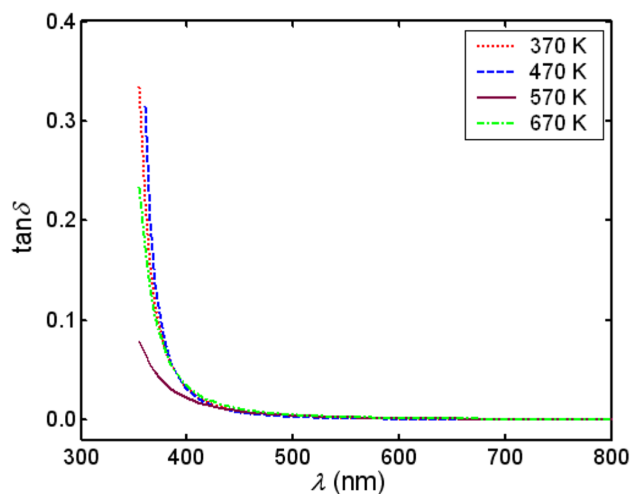

Fig. 12 The curves of tanδ for the films deposited at different substrate temperatures

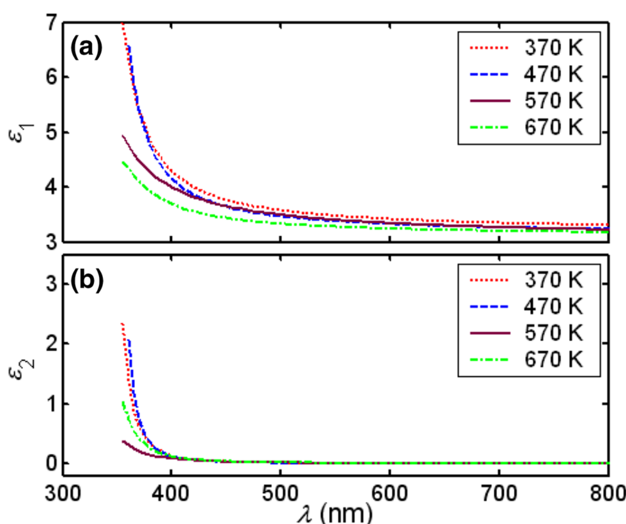

Fig. 11 The curves of ε_1 and ε_2 for the films deposited at different substrate temperatures

decrease with increasing wavelength λ, and the ε_1 is significantly larger than the ε_2 for all the samples. Corresponding to the substrate temperatures of 370, 470, 570 and 670 K, the values of ε_1 and ε_2 in the visible range are observed to be 4.304–3.309, 1.349×10^{-1}–2.957×10^{-4}; 4.155–3.235, 1.291×10^{-1}–2.186×10^{-4}; 4.017–3.226, 8.817×10^{-2}–8.871×10^{-4}; and 3.709–3.178, 1.261×10^{-1}–1.169×10^{-3}, respectively.

The dissipation factor (tanδ) of the deposited films were determined by the following relation [65]:

$$\tan\delta = \frac{\mathrm{Im}(\varepsilon)}{\mathrm{Re}(\varepsilon)} = \frac{\varepsilon_2}{\varepsilon_1} \tag{10}$$

Figure 12 gives the dependence of tanδ on wavelength λ for GMZO samples deposited at different substrate temperatures. As can be seen, the variation of tanδ follows the same trend as k and the tanδ value decreases monotonically with the increase of wavelength λ beyond 400 nm. In the visible range, the tanδ values are found to be 3.173×10^{-2}–8.938×10^{-5}, 3.081×10^{-2}–6.586×10^{-5}, 2.201×10^{-2}–2.725×10^{-4} and 3.449×10^{-2}–3.646×10^{-4} for the GMZO thin films deposited at the substrate temperatures of 370, 470, 570 and 670 K, respectively.

4 Conclusions

In summary, the transparent conductive GMZO thin films were deposited on glass substrates by magnetron sputtering technique. The effect of substrate temperature on the crystallinity, microstructure, morphology and optoelectronic properties of the thin films was investigated. The XRD patterns indicate that all the GMZO thin films have a hexagonal wurtzite type crystal structure and a (002) preferred orientation with the c-axis perpendicular to the substrate. The structural and optoelectronic properties of the thin films are found to be dependent on the substrate temperature. The smallest dislocation density (3.69×10^{14} lines m^{-2}), the minimum lattice strain (1.10×10^{-3}), the lowest electrical resistivity (1.62×10^{-3} Ω cm), the maximum average visible transmittance (88.63%) and the highest figure of merit (5.11×10^{3} Ω^{-1} cm^{-1}) are obtained when the substrate temperature is 570 K. The optical parameters such as refractive index, extinction coefficient, dielectric constant and dissipation factor were determined using optical characterization methods, and the dispersion behaviour of refractive index was analyzed by the single electronic oscillator model. It

is observed that the refractive index dispersion curves of the thin films obey the single electronic oscillator model. In addition, the optical energy gaps of the thin films were calculated by means of Tauc's relation and observed to be in the range of 3.34–3.55 eV. The results suggest that the substrate temperature is one of the most important deposition parameters to affect the microstructure and optoelectronic properties of GMZO thin films.

Acknowledgements This work was supported by the Fundamental Research Funds for the Central Universities (CZP17002, CZW14019), South-Central University for Nationalities. The authors would like to thank the reviewers and editors for several helpful comments.

References

1. Y.S. Song, N.J. Seong, K.J. Choi et al., Thin Solid Films **546**(1), 271–274 (2013)
2. Z. Zhong, H. Kang, Z. Lu et al., J. South-Cent. Univ. Natl. (Nat. Sci. Ed.) **36**(1), 64–70 (2017)
3. N. Yamamoto, H. Makino, S. Osone et al., Thin Solid Films **520**(12), 4131–4138 (2012)
4. S. Chen, J. South-Cent. Univ. Natl. (Nat. Sci. Ed.) **33**(2), 57–62 (2014)
5. J.-L. Wu, H.-Y. Lin, B.-Y. Su et al., J. Alloy. Compd. **592**(1), 35–41 (2014)
6. C.Y. Park, J.H. Lee, B.H. Choi, Org. Electron. **14**(12), 3172–3179 (2013)
7. H. Long, Z. Zhong, J. Gu et al., J. South-Cent. Univ. Natl. (Nat. Sci. Ed.) **36**(1), 71–75 (2017)
8. M. Hjiri, L.E. Mir, S.G. Leonardi et al., Sensor. Actuat. B **196**(1), 413–420 (2014)
9. J. Hu, Y. Zhou, H. Liu et al., J. South-Cent. Univ. Natl. (Nat. Sci. Ed.) **29**(2), 6–10 (2010)
10. A. Barhoumi, G. Leroy, B. Duponchel et al., Superlattice. Microstruct. **82**(1), 483–498 (2015)
11. Z. Zhong, J. Gu, X. He et al., J. South-Cent. Univ. Natl. (Nat. Sci. Ed.) **28**(4), 33–37 (2009)
12. S. Suzuki, T. Miyata, M. Ishii et al., Thin Solid Films **434**(1–2), 14–19 (2003)
13. S.D. Kirbey, R.B. Van Dover, Thin Solid Films **517**(6), 1958–1960 (2009)
14. A. Suresh, P. Wellenius, A. Dhawan et al., Appl. Phys. Lett. **90**(12), 123512–123514 (2007)
15. R. Ebrahimifard, M.R. Golobostanfard, H. Abdizadeh, Appl. Surf. Sci. **290**(1), 252–259 (2014)
16. L. Zhang, J. Huang, J. Yang et al., Mater. Sci. Semicond. Process **42**(Part 3), 277–282 (2016)
17. D. Fang, K. Lin, T. Xue et al., J. Alloy. Compd. **589**(1), 346–352 (2014)
18. A. Davoodi, M. Tajally, O. Mirzaee et al., J. Alloy. Compd. **657**(1), 296–301 (2016)
19. Z. Zhong, T. Zhang, H. Wang, J. South-Cent. Univ. Natl. (Nat. Sci. Ed.) **32**(1), 58–64 (2013)
20. K. Zheng, L. Gu, D. Sun et al., Mater. Sci. Eng. B **166**(1), 104–107 (2010)
21. T. Makino, K. Tamura, C.H. Chia et al., Phys. Stat. Sol. B **229**(3), 853–857 (2002)
22. L.-H. Cheng, L.-Y. Zheng, L. Meng et al., Ceram. Int. **38**(Supplement 1), s457–s461 (2012)
23. G.G. Valle, P. Hammer, S.H. Pulcinelli et al., J. Eur. Ceram. Soc. **24**(6), 1009–1013 (2004)
24. H. Mondragón-Suárez, A. Maldonado, L. de la Olvera et al., Appl. Surf. Sci. **193**(1–4), 52–59 (2002)
25. P. Singh, A. Kaushal, D. Kaur, J. Alloy. Compd. **471**(1–2), 11–15 (2009)
26. X. He, L. Xiong, J. South-Cent. Univ. Natl. (Nat. Sci. Ed.) **30**(2), 70–73 (2011)
27. J. Kim, J.H. Yun, S.W. Jee et al., Mater. Lett. **65**(4), 786–789 (2011)
28. J.P. Kar, S. Kim, B. Shin et al., Solid-State Electron. **54**(11), 1447–1450 (2010)
29. A. Zhou, H. Liu, Y. Yuan, J. Vacuum Sci. Technol. **32**(4), 974–977 (2012)
30. S. Chen, S. Wei, J. South-Cent. Univ. Natl. (Nat. Sci. Ed.) **34**(3), 72–78 (2015)
31. J. Mass, P. Bhattacharya, R.S. Katiyar, Mater. Sci. Eng. B **103**(1), 9–15 (2003)
32. F. Sun, S. Hui, J. South-Cent. Univ. Natl. (Nat. Sci. Ed.) **28**(2), 10–13 (2009)
33. X. Yu, J. Ma, F. Ji et al., Appl. Surf. Sci. **239**(2), 222–226 (2005)
34. I. Chambouleyron, S.D. Ventura, E.G. Birgin et al., J. Appl. Phys. **92**(6), 3093–3102 (2002)
35. E.G. Birgin, I. Chambouleyron, J.M. Martínez, J. Comput. Phys. **151**(2), 862–880 (1999)
36. J. Chen, D. Chen, J. He et al., Appl. Surf. Sci. **255**(23), 9413–9419 (2009)
37. Z.B. Ayadi, L.E. Mir, K. Djessas et al., Mater. Sci. Eng. C **28**(5–6), 613–617 (2008)
38. T. Huang, C. Li, J. Wu et al., J. South-Cent. Univ. Natl. (Nat. Sci. Ed.) **32**(3), 5–7 (2013)
39. S. Li, H. Yang, W. Wang et al., Mater. Rev. B **28**(10), 6–10 (2014)
40. K. Mageshwari, R. Sathyamoorthy, Mater. Sci. Semicond. Process **16**(2), 337–343 (2013)
41. J. Gu, Z. Lu, L. Long et al., J. South-Cent. Univ. Natl. (Nat. Sci. Ed.) **35**(2), 91–96 (2016)
42. D. Briggs, M.P. Seah, *Practical Surface Analysis by Auger and X-ray Photoelectron Spectroscopy*. (Wiley, New York, 1983)
43. Z.Z. You, J.Y. Dong, Vacuum **81**(7), 819–825 (2007)
44. C. Li, B. Yang, L. Qian et al., Optoelectron. Lett. **7**(6), 0431–0436 (2011)
45. Z. Huang, X. Liu, L. Wu et al., J. South-Cent. Univ. Natl. (Nat. Sci. Ed.) **35**(1), 17–22 (2016)
46. P.P. Sahay, S. Tewari, R.K. Nath, Cryst. Res. Technol. **42**(3), 723–729 (2007)
47. J. Gu, Z. Zhong, X. He et al., J. South-Cent. Univ. Natl. (Nat. Sci. Ed.) **28**(3), 30–33 (2009)
48. Z.Z. You, G.J. Hua, Y.C. Yong et al., Cryst. Res. Technol. **47**(10), 1039–1046 (2012)
49. S. Chen, C. Lan, J. South-Cent. Univ. Natl. (Nat. Sci. Ed.) **35**(2), 97–102 (2016)
50. L. de la Olvera, A. Maldonado, R. Asomoza et al., J. Mater. Sci.: Mater. Electron. **11**(5), 383–387 (2000)
51. X.-Y. Li, H.-J. Li, Z.-J. Wang et al., Opt. Commun. **282**(2), 247–252 (2009)
52. C.Y. Tsay, C.W. Wu, C.M. Lei et al., Thin Solid Films **519**(5), 1516–1520 (2010)
53. S.B. Chen, S. Wei, X. He et al., J. South-Cent. Univ. Natl. (Nat. Sci. Ed.) **28**(1), 43–46 (2009)
54. S.R. Aghdaee, V. Soleimanian, B. Tayebi, Superlattice. Microstruct. **51**(1), 149–162 (2012)
55. Q.-B. Ma, Z.-Z. Ye, H.-P. He et al., J. Cryst. Growth **304**(1), 64–68 (2007)
56. Q.B. Ma, Z.Z. Ye, H.P. He et al., Mater. Sci. Semicond. Process **10**(4–5), 167–172 (2007)
57. M. Lv, X. Xiu, Z. Pang et al., Appl. Surf. Sci. **252**(5), 2006–2011 (2005)

58. J. Gu, L. Long, Z. Lu et al., J. South-Cent. Univ. Natl. (Nat. Sci. Ed.) **34**(2), 68–73 (2015)
59. A.K. Singh, Optik **124**(15), 2187–2190 (2013)
60. Y. Yang, X.W. Sun, B.J. Chen et al., Thin Solid Films **510**(1–2), 95–101 (2006)
61. J. Gu, L. Long, C. Lan et al., J. South-Cent. Univ. Natl. (Nat. Sci. Ed.) **33**(4), 78–84 (2014)
62. D.R. Sahu, J.L. Huang, Sol. Energy Mater. Sol. Cells **93**(11), 1923–1927 (2009)
63. S. Aksoy, Y. Caglar, S. Ilican et al., J. Alloy. Compd. **512**(1), 171–178 (2012)
64. M. Zribi, M. Kanzari, B. Rezig, Mater. Lett. **60**(1), 98–103 (2006)
65. J.I. Pankove, *Optical Processes in Semiconductors*. (Dover Publications, New York, 1975)